

Long-Range Surface Plasmon Resonance Imaging for Bioaffinity Sensors

Alastair W. Wark, Hye Jin Lee, and Robert M. Corn*

Department of Chemistry, University of California—Irvine, Irvine, California 92697

A novel bioaffinity sensor based on surface plasmon resonance (SPR) imaging measurements of a multiple-layered structure that supports the generation of long-range surface plasmons (LRSPs) at the water–metal interface is reported. LRSPs possess longer surface propagation lengths, higher electric field strengths, and sharper angular resonance curves than conventional surface plasmons. LRSPR imaging is a version of SPR imaging that requires a symmetric dielectric arrangement around the gold thin film. This arrangement is created using an SF10 prism/Cytop/gold/water multilayer film structure where Cytop is an amorphous fluoropolymer with a refractive index very close to that of water. LRSPR imaging experiments are performed at a fixed incident angle and lead to an enhanced response for the detection of surface binding interactions. As an example, the hybridization adsorption of a 16-mer single-stranded DNA (ssDNA) onto a two-component ssDNA array was monitored with LRSPR imaging. The ssDNA array was created using a new fabrication technology appropriate for the LRSPR multilayers.

Long-range surface plasmons (LRSPs) are surface electromagnetic waves that can be created on thin metallic films imbedded between two identical dielectrics. Compared with conventional surface plasmons, LRSPs have longer surface propagation lengths, higher surface electric field strengths, and narrower angular resonance curves.^{1–8} The existence of LRSPs was first predicted¹ and then demonstrated² in the early 1980s, and subsequent studies have shown that LRSPs can be created in several different types of multiple-layered structures.^{3–7} However, due to the relative difficulty in fabricating structures that support LRSPs, long-range surface plasmon resonance (LRSPR) has been used to date only once to detect changes in the bulk refractive index of a material,⁸ and never for thin-film characterization or bioaffinity measurements.

SPR imaging has been used previously by several groups to monitor bioaffinity interactions in an array format.^{9–15} Can LRSPs also be used in an imaging format? In this paper, we describe a simple method for creating structures that support LRSPs at water–metal interfaces. The existence of LRSPs is verified by in situ scanning angle reflectivity measurements. Using a new array fabrication technology, we create a two-component single-stranded DNA (ssDNA) array and demonstrate that LRSPR imaging measurements can be used to detect biomolecular interactions with an enhanced sensitivity as compared with regular SPR imaging.

EXPERIMENTAL SECTION

Materials. 11-Mercaptoundecylamine (MUAM; Dojindo) and sulfosuccinimidyl 4-(*N*-maleimidomethyl)cyclohexane-1-carboxylate (SSMCC; Pierce) were used as received. Absolute ethanol and Millipore-filtered water were used for rinsing and for making solutions. All DNA oligonucleotides were commercially obtained from IDT (Integrated DNA Technologies). 5'-Thiol modifier C6 was used for 5'-thiol-modified DNA oligonucleotides and was deprotected as outlined by Glen Research Corp (<http://www.glenres.com>). Each DNA oligonucleotide was purified by reversed-phase binary gradient elution HPLC (Shimadzu SCL-10AVP), and DNA concentrations were verified with an HP8452A UV–visible spectrophotometer. The thiol-modified DNA sequence used contained a T15 spacer and is as follows: **D**₁, 5' HS(CH₂)₆(T)₁₅-GTC ATT GCG ACT AGT G; and **D**₂, 5' HS(CH₂)₆(T)₁₅GTG TTA GCC TCA AGT G. The DNA complementary oligonucleotides were used as received from IDT with HPLC purification. The 16-mer complementary to probe **D**₂ was 5' CAC TTG AGG CTA ACA C. All DNA hybridization experiments were conducted at room temperature in a buffer solution (pH 7.4) of 20 mM phosphate, 5 mM MgCl₂, 100 mM NaCl, and 1 mM EDTA.

LRSPR Chip Fabrication. Square SF10 glass substrates (18 × 18 mm; Schott Glass) were cleaned and spin-coated at room temperature with a stock solution of 9% Cytop (CTL-809M; M-grade; Asahi Glass Co.) dissolved in CTL-180 solvent (Asahi Glass Co.). The substrate was then baked at 70 °C for 40 min

* To whom correspondence should be addressed. E-mail: rcorn@uci.edu.

- (1) Sarid, D. *Phys. Rev. Lett.* **1981**, *47*, 1927–1930.
- (2) Quail, J. C.; Rako, J. G.; Simon, H. J. *Opt. Lett.* **1983**, *8*, 377–379.
- (3) Matsubara, K.; Kawata, S.; Minami, S. *Opt. Lett.* **1990**, *15*, 75–77.
- (4) Yang, F.; Bradberry, G. W.; Sambles, J. R. *Phys. Rev. Lett.* **1991**, *66*, 2030–2032.
- (5) Kessler, M. A.; Hall, E. A. H. *Thin Solid Films* **1996**, *272*, 161–169.
- (6) Lyndin, N. M.; Salakhutdinov, I. F.; Sychugov, V. A.; Usievich, B. A.; Pudonin, F. A.; Parriaux, O. *Sens. Actuators, B* **1999**, *54*, 37–42.
- (7) Toyama, S.; Doumae, N.; Shoji, A.; Ikariyama, Y. *Sens. Actuators, B* **2000**, *65*, 32–34.
- (8) Nenninger, G. G.; Tobiska, P.; Homola, J.; Yee, S. S. *Sens. Actuators, B* **2001**, *74*, 145–151.

- (9) Smith, E. A.; Corn, R. M. *Appl. Spectrosc.* **2003**, *57*, 320A–332A.
- (10) Wilkop, T.; Wang, Z.; Cheng, Q. *Langmuir* **2004**, *20*, 11141–11148.
- (11) Kanda, V.; Kariuki, J. K.; Harrison, D. J.; McDermott, M. T. *Anal. Chem.* **2004**, *76*, 7257–7262.
- (12) Kyo, M.; Yamamoto, T.; Motohashi, H.; Kamiya, T.; Kuroita, T.; Tanaka, T.; Engel, J. D.; Kawakami, B.; Yamamoto, M. *Genes Cells* **2004**, *9*, 153–164.
- (13) Shumaker-Parry, J. S.; Campbell, C. T. *Anal. Chem.* **2004**, *76*, 907–917.
- (14) Arena, G.; Contino, A.; Longo, E.; Sgarlata, C.; Spoto, G.; Zitob, V. *Chem. Commun.* **2004**, 1812–1813.
- (15) Lee, H. J.; Yan, Y.; Marriott, G.; Corn, R. M. *J. Physiol.* **2005**, *563*, 61–71.

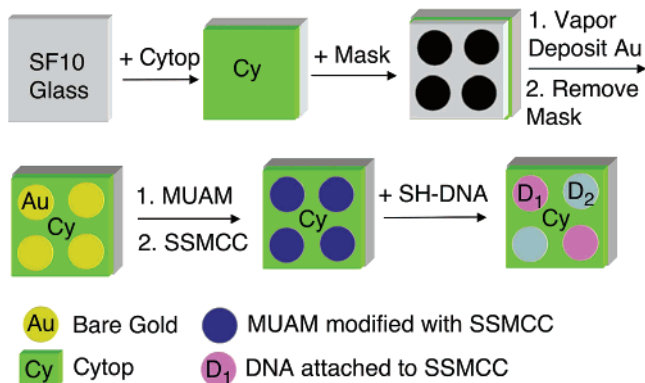


Figure 1. Schematic overview of the steps involved in the preparation of an LRSPR chip array for DNA binding studies using SPR imaging.

followed by 1 h at 190 °C. Gold films were vapor-deposited onto the Cytop-coated SF10 glass with a Denton DV-502A metal evaporator. A thin (1 nm) chromium underlayer was used to enhance the adhesion of gold. The Cytop thickness was measured by theoretically fitting in situ scanning angle SPR data of chips prepared with a known gold thickness. This procedure was repeated over a range of different spin rates to calibrate the Cytop film deposition conditions as well as characterize the corresponding SPR resonance curve profiles. For the Cytop film thickness specifically reported in this work, an initial spin rate of 500 rpm was applied for 10 s before quickly ramping to 2500 rpm and holding for 45 s. The steps involved in the preparation of the LRSPR chip array for DNA binding measurements using LRSPR imaging are summarized in Figure 1. (I) A Cytop thin film was deposited onto an SF10 glass slide as described above. (II) A mask was used during deposition to create a uniform array of gold spots with a diameter of 700 μm and edge-to-edge spacing of 550 μm . (III) A gold spotted array was immersed in a 1 mM ethanolic solution of MUAM for at least 2 h to form a self-assembled amine-terminated alkanethiol monolayer. (IV) The chip was washed with ethanol and water and dried under a steam of nitrogen. (V) A 1 mM solution of the heterobifunctional linker, SSMCC (in 100 mM TEA, pH 7), was spotted onto the amine-terminated MUAM array elements. (VI) This thiol-reactive maleimide-terminated surface was spotted with 5'-thiol-modified DNA and allowed to covalently attach overnight. After hybridization, the single stranded DNA (ssDNA) surface could be regenerated by washing with 8 M urea. This cycle could be repeated up to 20 times. The surface coverage of the ssDNA monolayer was estimated to be $\sim 1.0 \times 10^{12}$ molecules/ cm^2 . The conventional SPR chip arrays used for comparison purposes were fabricated in a manner identical to that described above with a gold thickness of 45 nm in the absence of a Cytop layer.

Scanning Angle SPR Measurements. The scanning angle SPR apparatus was composed of a 1-mW, 814-nm diode laser (Melles Griot) with the reflectivity of the p-polarized light measured as a function of the incident angle. The angle resolution of our setup was $\pm 0.0025^\circ$. As detailed elsewhere,¹⁶ the Kretschmann configuration was used with the SPR chip in optical contact with a hemispherical SF10 prism via index matching fluid ($n = 1.730$; Cargille). Experimental results were then analyzed with an N-phase Fresnel calculation.¹⁷

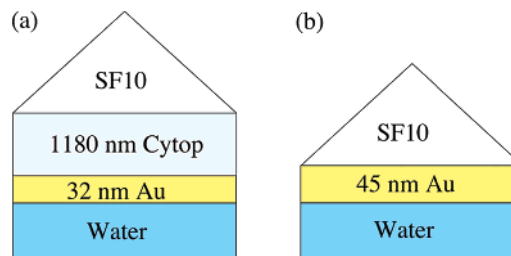


Figure 2. Schematic of multilayer chip/prism assemblies used for the excitation of long-range (a) and conventional (b) surface plasmons at the gold sensing surface.

SPR Imaging Measurements. An SPR imager apparatus (GWC Technologies) using excitation from an incoherent light source as previously described⁹ was used to detect the hybridization adsorption of complementary DNA in solution to surface-immobilized DNA probes. SPR imaging measures the change in percent reflectivity of p-polarized collimated white light at a fixed angle caused by the adsorption or desorption of biomolecules onto the surface. The sample prism assemblies used in both conventional and long-range experiments are compared in Figure 2. Reflected light from either assembly was passed through a band-pass filter centered at 830 nm and collected with a CCD camera. Complementary DNA solutions were introduced to the sample surface and allowed to react before the array surface was washed with buffer prior to collecting an SPR image. The same instrument setup was used for both the LRSPR and the conventional SPR chips, thus allowing a direct comparison.

RESULTS AND DISCUSSION

Long-Range Surface Plasmon Resonance. LRSPR requires dielectric layers with similar refractive indices on either side of a thin, continuous noble metal film. Figure 2a shows a schematic of the multilayer structure used to create LRSPs at the gold-water interface. A 1180-nm layer of the fluoropolymer Cytop ($n = 1.34$) is created by spin coating on an SF10 glass slide that can be optically attached to an SF10 prism. A 32-nm layer of gold is then vapor deposited onto the Cytop film. The Cytop is used in the four-phase LRSPR configuration SF10/Cytop (1180 nm)/gold (32 nm)/water to create the symmetric dielectric condition for the gold film. Also shown in Figure 2b is the three-phase configuration of SF10/gold (45 nm)/water used in conventional SPR. For both chips, a 1-nm chromium layer was first deposited in order to promote gold adhesion. Although not shown, this ultrathin Cr layer was included in both of the multilayer dielectric models used to analyze the SPR resonance curve shapes.

To demonstrate that LRSPs could be created with these multilayer films, a combination of scanning angle SPR measurements and Fresnel calculations were performed. The scanning angle SPR was carried out using a previously described setup,¹⁶ and the multiphase Fresnel calculations were obtained from the method of Hansen¹⁷ using programs available on our web site (<http://www.corninfo.ps.uci.edu/>). Figure 3 shows both the SPR reflectivity curve obtained for a conventional chip configuration (\diamond) and the reflectivity curve for a LRSPR chip (\circ). The circles and diamonds are data points, and the solid line is the theoretical

(16) Frutos, A. G.; Corn, R. M. *Anal. Chem.* **1999**, *70*, 449A–455A.

(17) Hansen, W. N. *J. Opt. Soc. Am.* **1968**, *58*, 380–390.

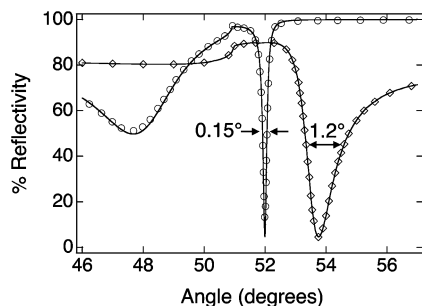


Figure 3. SPR reflectivity curves of p-polarized light as a function of incident angle, for a conventional SF10 glass/45-nm Au/water assembly (\diamond) and a SF10 glass/1180-nm Cytop/32-nm Au/water LRSPR design (\circ). Measurements were performed at an excitation wavelength of 814 nm. The arrows indicate the fwhm. The solid lines show the results of a theoretical fit to the data using a multiple-phase Fresnel calculation. Refractive indices (n) used in the calculation: $n(\text{SF10}) = 1.711$, $n(\text{Cytop}) = 1.336$, $n(\text{Cr}) = 3.186 + 3.47i$, $n(\text{Au}) = 0.185 + 5.11i$, and $n(\text{H}_2\text{O}) = 1.328$.

curve from the Fresnel calculation. Comparison of both measurements in Figure 3 shows the positions of the SPR and LRSPR resonances to be very different. Furthermore, the width of the SPR curve at half-maximum height (fwhm) for the regular chip design is 1.2° while the resonance curve on the long-range chip is much sharper with a more symmetric shape and a fwhm of 0.15° . The narrow resonance in the LRSPR reflectivity curve is associated with the excitation of an LRSP mode at the gold–water interface. Additionally, at angles prior to the critical angle (which is at $\sim 51^\circ$), the dip in the resonance curve is part of an interference pattern whose fringe spacing is dependent on the thickness of the Cytop layer.

The number, position, and depth of experimentally observed SP modes depend on the thickness of both the Cytop and gold thin-film layers. For a gold film of 50–75 nm, SP modes can be excited simultaneously at both the Cytop–gold and gold–water interfaces with varying efficiency, as the Cytop thickness is varied from 400 to 1200 nm. These two modes are observed experimentally as distinct peaks beyond the critical angle. The electric fields associated with these SP waves decay rapidly within the gold layer and do not overlap. However, as the gold layer becomes thinner (< 40 nm), the SP modes generated on opposite sides of the gold film couple to form a symmetric (long-range) and antisymmetric (short-range) pair. The result is a significant redistribution of the surface plasmon electric field intensity across the multilayer structure, with a larger fraction of the electric field existing in the lossless dielectrics outside the metal film. The short-range mode decays rapidly within the gold film, and only the long-range (LRSP) mode is observed experimentally. Compared with conventional surface plasmons, the higher field intensities at the gold surface associated with the LRSP mode correspond to a much longer propagation length of the LRSP wave. At 814 nm, the propagation length of SP modes has been measured¹⁸ to approach $25 \mu\text{m}$. Since there is a reciprocal relationship between the propagation length and the SPR curve fwhm,¹⁹ the results in Figure 3 suggest an 8-fold increase in the propagation length for the LRSP

(18) Berger, C. E. H.; Kooyman, R. P. H.; Greve, J. *Rev. Sci. Instrum.* **1994**, *65*, 2829–2836.

(19) Raether, H. *Surface Plasmons on Smooth and Rough Surfaces and on Gratings*; Springer-Verlag: Berlin, 1988.

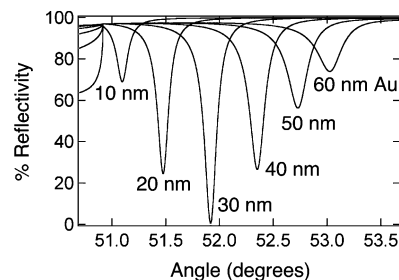


Figure 4. Theoretical calculations at an excitation wavelength of 814 nm showing the dependence of the in situ LRSPR resonance curve shape as a function of gold thickness at a fixed Cytop thickness of 1180 nm. The optimum gold thickness for SPR imaging measurements is close to 30 nm.

mode to $\sim 200 \mu\text{m}$. Additionally, the penetration or probe depth of the LRSPR mode into the bulk water phase will be longer than the 200 nm typical of conventional surface plasmon waves.

The theoretical dependence of the LRSPR curve shape on gold film thickness for a fixed Cytop thickness of 1180 nm is shown in Figure 4. An LRSP mode is observed at all gold thicknesses of 60 nm and below. These calculations show that the LRSPR curve reflectivity is lowest at a thickness of 30 nm. Additionally, the fwhm of the resonance curve decreases as the gold thickness is reduced, reaching a constant value of $\sim 0.13^\circ$ below 30 nm. This indicates that the optimum gold thickness for surface binding studies is close to 30 nm since the plasmon electric field intensity will be highest with maximum coupling of the incident excitation light. SPR imaging measurements are performed at an optimum angle just off the minimum resonance angle where the slope of the SPR curve is at its steepest. Therefore, maximum image contrast as well as a greater dynamic range is attained at a gold thickness close to 30 nm. On selecting a different Cytop thickness, the corresponding optimum gold film thickness will vary.

Bioaffinity Sensing Using LRSPR Imaging. The advantages of LRSPR compared to regular SPR for the detection of bioaffinity interactions in an imaging format was demonstrated by monitoring the hybridization adsorption of a 16-mer ssDNA onto a two-component ssDNA array. An LRSPR array was created by vapor depositing gold onto a Cytop-coated SF10 glass slide through a mask, resulting in a set of uniform gold spots (see Figure 1). Since the propagation length of the long-range surface plasmon is on the order of $200 \mu\text{m}$ at the imaging wavelength of 830 nm, a spot size with a diameter of $700 \mu\text{m}$ was chosen. A two-component array composed of two noninteracting DNA probe molecules was fabricated by the surface attachment of thiol-modified oligonucleotides onto alkanethiol-modified gold spots via the attachment chemistry described previously.²⁰ An LRSPR reflectivity difference image (see Figure 5a) was obtained by subtracting images taken before and after exposure of the array to a 500 nM solution of target DNA that is complementary only to the D_2 probe. Specific binding resulting in an increase of difference percent reflectivity ($\Delta\%R$) is clearly observed at the D_2 array elements shown by the schematic in Figure 5b with no change in signal occurring at the D_1 probe elements.

Quantitative analysis of the SPR difference images was performed by analyzing line profiles (see Figure 5c) and integrating

(20) Nelson, B. P.; Grimsrud, T. E.; Liles, M. R.; Goodman, R. M.; Corn, R. M. *Anal. Chem.* **2001**, *73*, 1–7.

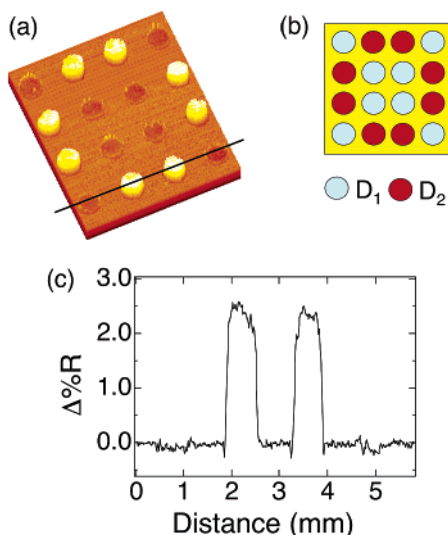


Figure 5. SPR difference image (a) obtained by subtracting images taken before and after exposure to a 500 nM solution of ssDNA complementary only to the D_2 probe array elements defined in (b). The LRSPR chip consisted of 1180-nm Cytop and 32-nm Au layers. A line profile (c) was taken across the image, as drawn on the difference image, to extract quantitative information. The line profile shows an increase in difference percent reflectivity corresponding to the specific hybridization adsorption of DNA at the D_2 probe elements only. The array was regenerated by washing with 8 M urea to denature the surface.

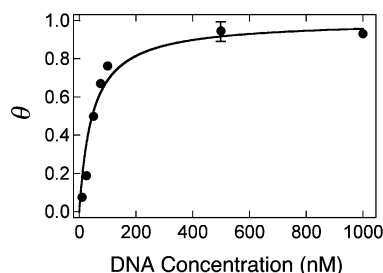


Figure 6. Relative surface coverage (fraction of occupied surface sites, θ) as determined by measuring the difference percent reflectivity ($\Delta\%R$) as a function of complement DNA concentration in the solution. An LRSPR chip was used with the same design as described in Figure 2. The solid line represents a Langmuir isotherm fit to the data. From this fit, a value of $K_{\text{Ads}} = 2.2 (\pm 0.4) \times 10^7 \text{ M}^{-1}$ was determined.

over the cross-sectional area corresponding to DNA binding. In this case, the change in $\Delta\%R$ obtained on averaging over a number of repeat measurements was $2.0 (\pm 0.2)\%$. Theory predicts that LRSPR imaging should be better in the near-infrared (as in conventional SPR imaging²¹). Specifically, for the Cytop and gold thicknesses described in Figure 2, an improvement of $\sim 40\%$ compared to regular SPR imaging is predicted for LRSPR imaging. Repeated measurements over a series of DNA concentrations for both LRSPR chips (see Figure 6) and regular SPR chips (data not shown) showed an $\sim 20\%$ increase in the LRSPR $\Delta\%R$ signal. For example, using LRSPR, the hybridization-adsorption of a 5 nM 16-mer DNA sample can be easily observed, which is the detection limit in conventional SPR imaging. It is expected that further optimization such as reducing the angular spread of the incident white light source collimation optics will result in further signal enhancement.

The binding strength of the ssDNA to the ssDNA microarray was determined through the concentration dependence of the LRSPR imaging signal. Figure 6 plots the fractional surface coverage (θ) versus DNA concentration, where the solid line represents a Langmuir adsorption isotherm data fit, with a value for the equilibrium adsorption coefficient, K_{Ads} , of $2.2 (\pm 0.4) \times 10^7 \text{ M}^{-1}$. This value closely matches the adsorption coefficient of $1.9 (\pm 0.4) \times 10^7 \text{ M}^{-1}$ obtained for repeat measurements using a conventional SPR chip. These results establish that the LRSPR chip behaves quantitatively over the detection range measured where changes in the percent reflectivity can be linearly related to the surface coverage of adsorbed molecules.

CONCLUSIONS

These measurements represent the first successful demonstration of the application of long-range surface plasmons for biomolecular detection and for thin-film sensing in general. A multilayer structure was designed where, by controlling the relative thicknesses of the Cytop and gold film layers, much narrower angular resonance curves associated with the excitation of long-range surface plasmons were achieved. Crucial to the success of this measurement was the use of Cytop as an inert, optically transparent material whose refractive index matches closely to that of water. LRSPs are associated with higher electric field intensities at the gold sensing surface. However, one potential disadvantage of LRSPs for sensing in an imaging format could be that the longer propagation length reduces the lateral resolution of the image. As a result, a new fabrication approach was developed to create an LRSPR array consisting of a series of uniform gold spots whose size was greater than the LRSP propagation length. Finally, surface DNA hybridization adsorption studies demonstrated that LRSPR can be applied in an imaging format and is slightly more sensitive than conventional SPR imaging, yet still responds in a quantitative manner to changes in the surface coverage of adsorbed molecules. The amount of enhancement depends on the narrow resonance of the LRSPR curve. The difference between the 40% improvement predicted compared to the 20% experimentally observed is attributed to the difficulty in collimating the incident white light source to the level of precision required. Subsequent work will focus on improving both the collimation optics and the instrumentation as this will allow further optimization of the chip design since it is predicted that even narrower resonance curves can be achieved for thicker Cytop films (e.g., 1500-nm Cytop, 24-nm Au), which will lead to further signal enhancement.

ACKNOWLEDGMENT

This work was supported by grants from NSF (CHE-0133151), NSF-SBIR (0319219), and NIH (2R01C7M059622-04) and a start-up grant from the University of California, Irvine. We also thank Dr. V. Kodoyianni and Dr. T. Burland from GWC Technologies for their helpful discussions and assistance during the course of this work.

Received for review March 8, 2005. Accepted April 21, 2005.

AC050402V

(21) Nelson, B. P.; Frutos, A. G.; Brockman, J. M.; Corn, R. M., *Anal. Chem.* **1999**, *71*, 3928–3934.